

- ² *Beihang University, Beijing 100191, People's Republic of China*
- ³ *Beijing Institute of Petrochemical Technology, Beijing 102617, People's Republic of China*
- ⁴ *Bochum Ruhr-University, D-44780 Bochum, Germany*
- ⁵ *Carnegie Mellon University, Pittsburgh, Pennsylvania 15213, USA*
- ⁶ *Central China Normal University, Wuhan 430079, People's Republic of China*
- ⁷ *China Center of Advanced Science and Technology, Beijing 100190, People's Republic of China*
- ⁸ *COMSATS University Islamabad, Lahore Campus, Defence Road, Off Raiwind Road, 54000 Lahore, Pakistan*
- ⁹ *Fudan University, Shanghai 200443, People's Republic of China*
- ¹⁰ *G.I. Budker Institute of Nuclear Physics SB RAS (BINP), Novosibirsk 630090, Russia*
- ¹¹ *GSI Helmholtzcentre for Heavy Ion Research GmbH, D-64291 Darmstadt, Germany*
- ¹² *Guangxi Normal University, Guilin 541004, People's Republic of China*
- ¹³ *Guangxi University, Nanning 530004, People's Republic of China*
- ¹⁴ *Hangzhou Normal University, Hangzhou 310036, People's Republic of China*
- ¹⁵ *Helmholtz Institute Mainz, Johann-Joachim-Becher-Weg 45, D-55099 Mainz, Germany*
- ¹⁶ *Henan Normal University, Xinxiang 453007, People's Republic of China*
- ¹⁷ *Henan University of Science and Technology, Luoyang 471003, People's Republic of China*
- ¹⁸ *Huangshan College, Huangshan 245000, People's Republic of China*
- ¹⁹ *Hunan Normal University, Changsha 410081, People's Republic of China*
- ²⁰ *Hunan University, Changsha 410082, People's Republic of China*
- ²¹ *Indian Institute of Technology Madras, Chennai 600036, India*
- ²² *Indiana University, Bloomington, Indiana 47405, USA*
- ²³ *(A)INFN Laboratori Nazionali di Frascati, I-00044, Frascati, Italy; (B)INFN and University of Perugia, I-06100, Perugia, Italy*
- ²⁴ *(A)INFN Sezione di Ferrara, I-44122, Ferrara, Italy; (B)University of Ferrara, I-44122, Ferrara, Italy*
- ²⁵ *Institute of Modern Physics, Lanzhou 730000, People's Republic of China*
- ²⁶ *Institute of Physics and Technology, Peace Ave. 54B, Ulaanbaatar 13330, Mongolia*
- ²⁷ *Jilin University, Changchun 130012, People's Republic of China*
- ²⁸ *Johannes Gutenberg University of Mainz, Johann-Joachim-Becher-Weg 45, D-55099 Mainz, Germany*
- ²⁹ *Joint Institute for Nuclear Research, 141980 Dubna, Moscow region, Russia*
- ³⁰ *Justus-Liebig-Universitaet Giessen, II. Physikalisches Institut, Heinrich-Buff-Ring 16, D-35392 Giessen, Germany*
- ³¹ *KVI-CART, University of Groningen, NL-9747 AA Groningen, The Netherlands*
- ³² *Lanzhou University, Lanzhou 730000, People's Republic of China*
- ³³ *Liaoning Normal University, Dalian 116029, People's Republic of China*
- ³⁴ *Liaoning University, Shenyang 110036, People's Republic of China*
- ³⁵ *Nanjing Normal University, Nanjing 210023, People's Republic of China*
- ³⁶ *Nanjing University, Nanjing 210093, People's Republic of China*
- ³⁷ *Nankai University, Tianjin 300071, People's Republic of China*
- ³⁸ *Peking University, Beijing 100871, People's Republic of China*
- ³⁹ *Qufu Normal University, Qufu 273165, People's Republic of China*
- ⁴⁰ *Shandong Normal University, Jinan 250014, People's Republic of China*
- ⁴¹ *Shandong University, Jinan 250100, People's Republic of China*
- ⁴² *Shanghai Jiao Tong University, Shanghai 200240, People's Republic of China*
- ⁴³ *Shanxi Normal University, Linfen 041004, People's Republic of China*
- ⁴⁴ *Shanxi University, Taiyuan 030006, People's Republic of China*
- ⁴⁵ *Sichuan University, Chengdu 610064, People's Republic of China*
- ⁴⁶ *Soochow University, Suzhou 215006, People's Republic of China*
- ⁴⁷ *Southeast University, Nanjing 211100, People's Republic of China*
- ⁴⁸ *State Key Laboratory of Particle Detection and Electronics, Beijing 100049, Hefei 230026, People's Republic of China*
- ⁴⁹ *Sun Yat-Sen University, Guangzhou 510275, People's Republic of China*
- ⁵⁰ *Tsinghua University, Beijing 100084, People's Republic of China*
- ⁵¹ *(A)Ankara University, 06100 Tandogan, Ankara, Turkey; (B)Istanbul Bilgi University, 34060 Eyup, Istanbul, Turkey; (C)Uludag University, 16059 Bursa, Turkey; (D)Near East University, Nicosia, North Cyprus, Mersin 10, Turkey*
- ⁵² *University of Chinese Academy of Sciences, Beijing 100049, People's Republic of China*
- ⁵³ *University of Hawaii, Honolulu, Hawaii 96822, USA*
- ⁵⁴ *University of Jinan, Jinan 250022, People's Republic of China*
- ⁵⁵ *University of Manchester, Oxford Road, Manchester, M13 9PL, United Kingdom*
- ⁵⁶ *University of Minnesota, Minneapolis, Minnesota 55455, USA*
- ⁵⁷ *University of Muenster, Wilhelm-Klemm-Str. 9, 48149 Muenster, Germany*
- ⁵⁸ *University of Oxford, Keble Rd, Oxford, UK OX13RH*
- ⁵⁹ *University of Science and Technology Liaoning, Anshan 114051, People's Republic of China*
- ⁶⁰ *University of Science and Technology of China, Hefei 230026, People's Republic of China*
- ⁶¹ *University of South China, Hengyang 421001, People's Republic of China*
- ⁶² *University of the Punjab, Lahore-54590, Pakistan*
- ⁶³ *(A)University of Turin, I-10125, Turin, Italy; (B)University of Eastern*

Piedmont, I-15121, Alessandria, Italy; (C)INFN, I-10125, Turin, Italy

⁶⁴ Uppsala University, Box 516, SE-75120 Uppsala, Sweden

⁶⁵ Wuhan University, Wuhan 430072, People's Republic of China

⁶⁶ Xinyang Normal University, Xinyang 464000, People's Republic of China

⁶⁷ Zhejiang University, Hangzhou 310027, People's Republic of China

⁶⁸ Zhengzhou University, Zhengzhou 450001, People's Republic of China

^a Also at Bogazici University, 34342 Istanbul, Turkey

^b Also at the Moscow Institute of Physics and Technology, Moscow 141700, Russia

^c Also at the Functional Electronics Laboratory, Tomsk State University, Tomsk, 634050, Russia

^d Also at the Novosibirsk State University, Novosibirsk, 630090, Russia

^e Also at the NRC "Kurchatov Institute", PNPI, 188300, Gatchina, Russia

^f Also at Istanbul Arel University, 34295 Istanbul, Turkey

^g Also at Goethe University Frankfurt, 60323 Frankfurt am Main, Germany

^h Also at Key Laboratory for Particle Physics, Astrophysics and Cosmology, Ministry of Education; Shanghai Key Laboratory for Particle Physics and Cosmology; Institute of Nuclear and Particle Physics, Shanghai 200240, People's Republic of China

ⁱ Also at Key Laboratory of Nuclear Physics and Ion-beam Application (MOE) and Institute of Modern Physics, Fudan University, Shanghai 200443, People's Republic of China

^j Also at Harvard University, Department of Physics, Cambridge, MA, 02138, USA

^k Currently at: Institute of Physics and Technology, Peace Ave.54B, Ulaanbaatar 13330, Mongolia

^l Also at State Key Laboratory of Nuclear Physics and Technology,

Peking University, Beijing 100871, People's Republic of China

^m School of Physics and Electronics, Hunan University, Changsha 410082, China

(Dated: October 16, 2020)

We report the first measurement of the absolute branching fraction of the inclusive decay $\Lambda_c^+ \rightarrow K_S^0 X$. The analysis is performed using an e^+e^- collision data sample corresponding to an integrated luminosity of 567 pb^{-1} taken at $\sqrt{s} = 4.6 \text{ GeV}$ with the BESIII detector. Using eleven Cabibbo-favored $\bar{\Lambda}_c^-$ decay modes and the double-tag technique, this absolute branching fraction is measured to be $\mathcal{B}(\Lambda_c^+ \rightarrow K_S^0 X) = (9.9 \pm 0.6 \pm 0.4)\%$, where the first uncertainty is statistical and the second systematic. The relative deviation between the branching fractions for the inclusive decay and the observed exclusive decays is $(18.7 \pm 8.3)\%$, which indicates that there may be some unobserved decay modes with a neutron or excited baryons in the final state.

PACS numbers: 13.30.-a, 14.20.Lq, 14.65.Dw

The lightest charmed baryon Λ_c^+ was first observed in e^+e^- annihilation at the Mark II experiment [1]. Hadronic Λ_c^+ decays offer an ideal platform to understand both strong and weak interactions. Most branching fractions (BFs) of Λ_c^+ decays were previously measured relative to the BF of $\Lambda_c^+ \rightarrow pK^-\pi^+$ [2]. In recent years, the BESIII experiment reported a series of absolute measurements of exclusive decays of the Λ_c^+ baryon [3–10]. The precision of BFs for the known decay modes was significantly improved and some new decay modes were observed. Using the statistical isospin model [11], it is estimated that about 90% of the Λ_c^+ decay modes are now known. Measurements of the BFs for inclusive decays of the Λ_c^+ baryon are important to understand its decay mechanisms and indicate the size and type of unmeasured decays by comparing with the BFs for the corresponding exclusive decays.

The Cabibbo-favored (CF) decays of charmed mesons have been well studied [2]. However, the information of the CF decays of charmed baryons is relatively limited. The Λ_c^+ CF decays are dominantly modes involving Λ , Σ and \bar{K} in the final state. According to the statistical isospin model, the total BF of the observed and extrapolated CF decays of Λ_c^+ baryon is

$(83.2 \pm 4.9)\%$ [11]. Measurements of the BF of the inclusive decays will help to characterize Λ_c^+ CF decays. Recently, BESIII measured the absolute inclusive BF $\mathcal{B}(\Lambda_c^+ \rightarrow \Lambda X) = (38.2_{-2.2}^{+2.8} \pm 0.9)\%$ [12], which appears to be larger than the total observed and extrapolated BFs for exclusive Λ decays $(31.7 \pm 1.4)\%$ [11]. The total BF of exclusive \bar{K}^0/K^0 decays of Λ_c^+ is estimated to be $(22.4 \pm 0.9)\%$ by the statistical isospin model [11], as listed in Table I, while the total observed BF for decays to \bar{K}^0/K^0 only sum to $(16.1 \pm 0.8)\%$. Determining the absolute BF of inclusive Λ_c^+ decays to \bar{K}^0/K^0 will help to quantify the missing decay modes and test the predicted BFs of decay modes extrapolated by the statistical isospin model.

In this paper, we measure the absolute BF of the inclusive decay of the Λ_c^+ to K_S^0 ($\Lambda_c^+ \rightarrow K_S^0 X$) for the first time, where X indicates all possible particle combinations. This analysis uses 567 pb^{-1} of data [13] collected at the center-of-mass energy $\sqrt{s} = 4.6 \text{ GeV}$ with the BESIII detector. The measurement is performed using the double-tag (DT) technique [14], since there is no additional hadrons accompanying $\Lambda_c^+\bar{\Lambda}_c^-$ pair produced at this energy. First, the $\bar{\Lambda}_c^-$ baryons are reconstructed with exclusive hadronic decay modes which are called the

single-tag (ST) modes. Then the $\Lambda_c^+ \rightarrow K_S^0 X$ mode is reconstructed in the $\bar{\Lambda}_c^-$ recoiling side, called the signal mode or the DT mode. The ST $\bar{\Lambda}_c^-$ baryons are reconstructed including the following eleven hadronic decay modes: $\bar{p}K_S^0$, $\bar{p}K^+\pi^-$, $\bar{p}K_S^0\pi^0$, $\bar{p}K_S^0\pi^+\pi^-$, $\bar{p}K^+\pi^-\pi^0$, $\bar{\Lambda}\pi^-$, $\bar{\Lambda}\pi^-\pi^0$, $\bar{\Lambda}\pi^-\pi^+\pi^-$, $\bar{\Sigma}^0\pi^-$, $\bar{\Sigma}^-\pi^0$, and $\bar{\Sigma}^-\pi^+\pi^-$, with a total BF of $(35.0 \pm 0.7)\%$. Throughout this paper, charge-conjugate modes are implicitly assumed unless explicitly stated.

TABLE I. Observed and extrapolated BFs for exclusive \bar{K}^0/K^0 decays of Λ_c^+ CF decays [2, 11]. Here, observed BFs are referred from Particle Data Group (PDG) [2] and extrapolated BFs are referred from Ref. [11]. BFs of the \bar{K}^0/K^0 decay modes are obtained by doubling those quoted for K_S^0 decay modes. The total uncertainty is obtained as the sum in quadrature.

Mode	Value (%)	Mode	Value (%)
Observed BF		Extrapolated BF	
$p\bar{K}^0$	3.18 ± 0.16	$n\bar{K}^0\pi^+\pi^0$	3.07 ± 0.16
$p\bar{K}^0\pi^0$	3.94 ± 0.26	$p\bar{K}^0\pi^0\pi^0$	1.36 ± 0.07
$p\bar{K}^0\pi^+\pi^-$	3.20 ± 0.24	$n\bar{K}^0\pi^+\pi^+\pi^-$	0.14 ± 0.09
$n\bar{K}^0\pi^+$	3.64 ± 0.50	$p\bar{K}^0\pi^+\pi^-\pi^0$	0.22 ± 0.14
$p\bar{K}^0\eta$	1.60 ± 0.40	$n\bar{K}^0\pi^+\pi^0\pi^0$	0.10 ± 0.06
$\Lambda K^+\bar{K}^0$	0.57 ± 0.11	$p\bar{K}^0\pi^0\pi^0\pi^0$	0.03 ± 0.02
		$(\Sigma K)^+\bar{K}^0$	0.68 ± 0.34
		$\Xi^0 K^0\pi^+$	0.62 ± 0.06
Total	16.1 ± 0.8	Total	6.3 ± 0.4
Total		Total	22.4 ± 0.9

The BESIII detector is described in detail in Ref. [15]. It has an effective geometrical acceptance of 93% of 4 π . The cylindrical core of the BESIII detector consists of a small-cell, helium-based (40% He, 60% C₃H₈) multi-layer drift chamber (MDC), a plastic scintillator time-of-flight system (TOF), a CsI(Tl) electromagnetic calorimeter (EMC), and a muon system containing resistive plate chambers in the iron return yoke of a 1 T superconducting solenoid. The momentum resolution for charged tracks is 0.5% at a momentum of 1 GeV/c. Charged particle identification (PID) is accomplished by combining the energy loss (dE/dx) measurements in the MDC and flight times in the TOF. The photon energy resolution at 1 GeV is 2.5% in the barrel and 5% in the end caps.

A Monte Carlo (MC) simulation based on GEANT4 [16] includes the geometric description of the BESIII detector and its response. We generate high-statistics MC samples to study the background and estimate the detection efficiencies; initial-state radiation (ISR) [17] and final-state radiation [18] are also included in the MC simulation. $\Lambda_c^+\bar{\Lambda}_c^-$ pairs, $D_{(s)}^{(*)}\bar{D}_{(s)}^{(*)}X$ production, ISR production of ψ states, and continuum $q\bar{q}$ processes are simulated with generic MC samples generated using the KKMC generator [19]. The known decay modes are simulated with EVTGEN [20] using BFs taken from PDG [2], and the remaining unknown decays are simulated with the LUND-

CHARM model [21].

Charged tracks are detected in MDC. For prompt tracks, the polar angle (θ) is required to satisfy $|\cos\theta| < 0.93$, and the point of closest approach to the interaction point (IP) is required to be less than 10 cm in the beam direction and less than 1 cm in the transverse plane. Secondary tracks used to reconstruct K_S^0 or $\bar{\Lambda}$ candidates are subject to different IP requirements as detailed below. Particle identification (PID) for charged tracks combining the measurements of the energy loss dE/dx in the MDC and the flight time information is employed to calculate a likelihood $\mathcal{L}(h)$ for each hadron ($h = p, K, \text{ or } \pi$) hypothesis. Protons, kaons and pions are identified by requiring that the likelihood for the given hypothesis is larger than for both of the other two hypotheses.

Photon candidates are reconstructed by clustering electromagnetic calorimeter (EMC) crystal energies. The deposited energy is required to be greater than 25 MeV in the EMC barrel region ($|\cos\theta| < 0.80$) and 50 MeV in the EMC end cap region ($0.86 < |\cos\theta| < 0.92$). To eliminate showers from charged particles, the angle between the photon and the nearest charged track is required to be greater than 20°. Timing requirements are used to suppress electronic noise and energy deposits in the EMC unrelated to the event. π^0 candidates are reconstructed from photon pairs with an invariant mass in the range $0.115 < M_{\gamma\gamma} < 0.150$ GeV/ c^2 . A mass-constrained fit to the π^0 nominal mass [2] is performed to improve the momentum resolution.

K_S^0 and $\bar{\Lambda}$ candidates are reconstructed by combining pairs of oppositely charged tracks ($\pi^+\pi^-$ for K_S^0 and $\bar{p}\pi^+$ for $\bar{\Lambda}$) satisfying $|\cos\theta| < 0.93$ for the polar angle. The distance to the IP in the beam direction is required to be within 20 cm. No distance constraints in the transverse plane are required. Charged pions from these decays are not subjected to the PID requirement, while proton PID is applied in order to improve signal significance. The two charged tracks are constrained to originate from a common decay vertex by requiring the χ^2 of the vertex fit to be less than 100. Furthermore, the decay vertex is required to be separated from the IP by a distance of at least twice the uncertainty of the vertex fit. To select K_S^0 , $\bar{\Lambda}$, $\bar{\Sigma}^0$, and $\bar{\Sigma}^-$, the invariant mass of $\pi^+\pi^-$, $\bar{p}\pi^+$, $\bar{p}\pi^+\gamma$ and $\bar{p}\pi^0$ are required to be within (0.487, 0.511) GeV/ c^2 , (1.111, 1.121) GeV/ c^2 , (1.179, 1.203) GeV/ c^2 and (1.176, 1.200) GeV/ c^2 , respectively.

For the ST modes $\bar{p}K_S^0\pi^0$, $\bar{p}K_S^0\pi^+\pi^-$ and $\bar{\Sigma}^-\pi^+\pi^-$, background events containing a $\bar{\Lambda}$ are rejected by vetoing candidate events with $M(\bar{p}\pi^+)$ in the interval (1.110, 1.120) GeV/ c^2 . K_S^0 backgrounds for the ST modes $\bar{\Lambda}\pi^-\pi^+\pi^-$, $\bar{\Sigma}^-\pi^0$ and $\bar{\Sigma}^-\pi^+\pi^-$ are suppressed by requiring $M(\pi^+\pi^-)$ or $M(\pi^0\pi^0)$ to be outside of (0.480, 0.520) GeV/ c^2 . To remove $\bar{\Sigma}^-$ background in the ST mode $\bar{p}K_S^0\pi^0$, candidates within the range $1.170 < M(\bar{p}\pi^0) < 1.200$ GeV/ c^2 are excluded.

The quantities $M_{\text{BC}} = \sqrt{E_{\text{beam}}^2 - |\vec{p}_{\bar{\Lambda}_c^-}|^2}$ and $\Delta E = E_{\bar{\Lambda}_c^-} - E_{\text{beam}}$ are used to identify ST $\bar{\Lambda}_c^-$ candidates, where E_{beam} is the beam energy and $E_{\bar{\Lambda}_c^-}$ and $\vec{p}_{\bar{\Lambda}_c^-}$ are energy and momentum of the $\bar{\Lambda}_c^-$ candidate. To improve the signal purity, $|\Delta E|$ requirements corresponding to about three times the resolutions are imposed on $\bar{\Lambda}_c^-$ candidates; details are given in Table II. If there is more than one candidate per ST mode, the one with minimum $|\Delta E|$ is chosen. The $\bar{\Lambda}_c^-$ signals are clearly visible in the M_{BC} distributions of the eleven tag modes, as shown in Fig. 1. Peaking backgrounds are negligible according to MC studies [22]. Unbinned maximum likelihood fits to M_{BC} distributions are used to determine the ST yields for each tag mode, where the signal shape is described by the MC-simulated shape convolved with a Gaussian function to better match the resolution found in data, and the background shape is described by an ARGUS function [23]. The resultant ST yields in the signal region $2.282 < M_{\text{BC}} < 2.300$ GeV/ c^2 and the corresponding detection efficiencies are listed in Table II.

TABLE II. Requirements on ΔE , ST yields in data (N_i^{tag}), ST (ϵ_i^{tag}) and DT ($\epsilon_i^{\text{tag,sig}}$) efficiencies for the tag mode i . Uncertainties on N are statistical only, while uncertainties on efficiencies are due to the MC statistics. The quoted efficiencies do not include any BF's of subsequent decays.

Mode	ΔE (MeV)	N_i^{tag}	ϵ_i^{tag} (%)	$\epsilon_i^{\text{tag,sig}}$ (%)
$\bar{p}K_S^0$	(-20, 19)	1222±37	55.3±0.2	26.6±0.4
$\bar{p}K^+\pi^-$	(-20, 15)	6024±85	49.2±0.1	24.9±0.2
$\bar{p}K_S^0\pi^0$	(-30, 20)	498±29	18.9±0.1	8.7±0.2
$\bar{p}K_S^0\pi^+\pi^-$	(-20, 20)	376±24	15.5±0.1	7.1±0.2
$\bar{p}K^+\pi^-\pi^0$	(-30, 20)	1544±57	16.1±0.1	7.8±0.1
$\bar{\Lambda}\pi^-$	(-20, 20)	693±30	42.1±0.2	22.4±0.4
$\bar{\Lambda}\pi^-\pi^0$	(-30, 20)	1362±47	14.1±0.1	6.9±0.1
$\bar{\Lambda}\pi^-\pi^+\pi^-$	(-20, 20)	569±30	11.5±0.1	5.4±0.1
$\bar{\Sigma}^0\pi^-$	(-20, 20)	438±26	25.2±0.1	12.0±0.4
$\bar{\Sigma}^-\pi^0$	(-50, 30)	291±32	23.0±0.2	12.1±0.4
$\bar{\Sigma}^-\pi^+\pi^-$	(-30, 20)	1111±50	23.7±0.1	11.9±0.2

We select K_S^0 candidates among the remaining tracks on the recoiling side of the tagged $\bar{\Lambda}_c^-$. The selection criteria of K_S^0 are the same as those used in the ST $\bar{\Lambda}_c^-$ selection. If there is more than one K_S^0 candidate, the one with the minimum vertex fit χ^2 is selected for further analysis. Figure 2 (a) shows the distribution of M_{BC} versus the invariant mass of $\pi^+\pi^-$ pairs, $M(\pi^+\pi^-)$, of the accepted candidates for all eleven tag modes. There is a clear $\Lambda_c^+ \rightarrow K_S^0 X$ signal in the intersection of the K_S^0 and the ST $\bar{\Lambda}_c^-$ signal bands. A two-dimension (2D) fit to the distribution of M_{BC} versus $M(\pi^+\pi^-)$ is performed to determine the signal yield, as shown in Fig. 2. The signal function is the product of the $\bar{\Lambda}_c^-$ signal function and K_S^0 signal function. There are three kinds of background: the background peaking neither in the M_{BC} distribution nor in the $M(\pi^+\pi^-)$ distribution is described by the product

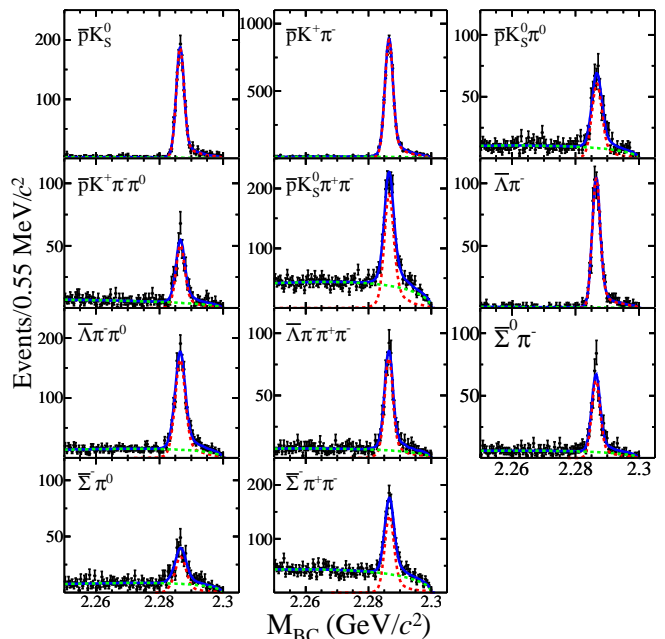


FIG. 1. Fits to the distributions of M_{BC} in data sample for different ST $\bar{\Lambda}_c^-$ modes, where the black dots with error bars are data, the blue lines are the fit results, the dashed red lines are signal shapes, and the dashed green lines are background shapes.

of $\bar{\Lambda}_c^-$ background function and K_S^0 background function; the background peaking around the $\bar{\Lambda}_c^-$ mass in the M_{BC} distribution is described by the product of $\bar{\Lambda}_c^-$ signal function and K_S^0 background function; the background peaking around the K_S^0 mass in the $M(\pi^+\pi^-)$ distribution is described by the product of $\bar{\Lambda}_c^-$ background function and K_S^0 signal function. The $\bar{\Lambda}_c^-$ signal is described by the MC-simulated shape convolved with a Gaussian function, while background is ARGUS function. The K_S^0 signal and background functions are described by a Gaussian function and a first-order polynomial, respectively. The signal yield is fitted to be 478 ± 27 , where the uncertainty is statistical.

The absolute BF $\mathcal{B}^{\text{sig}} = \mathcal{B}(\Lambda_c^+ \rightarrow K_S^0 X)$ is determined by

$$\mathcal{B}^{\text{sig}} = \frac{N^{\text{sig}}}{\mathcal{B}(K_S^0 \rightarrow \pi^+\pi^-) \cdot \sum_i N_i^{\text{tag}} \cdot \epsilon_i^{\text{tag,sig}} / \epsilon_i^{\text{tag}}}, \quad (1)$$

where $\epsilon_i^{\text{tag,sig}}$ is the DT efficiency for the tag mode i , as listed in Table II. The absolute BF of $\Lambda_c^+ \rightarrow K_S^0 X$ is calculated to be $\mathcal{B}(\Lambda_c^+ \rightarrow K_S^0 X) = (9.9 \pm 0.6)\%$, the uncertainty is statistical only. The reliability of the analysis method used in this work has been validated by analyzing the generic MC sample.

Systematic uncertainties from the ST side mostly cancel in the BF measurement with the DT method. Other systematic uncertainties for measuring $\mathcal{B}(\Lambda_c^+ \rightarrow K_S^0 X)$ are described below and summarized in Table III.

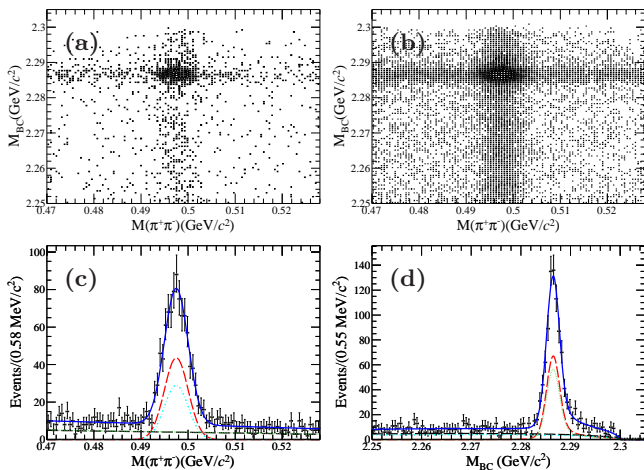


FIG. 2. [(a) and (b)] Distributions and [(c) and (d)] projections of M_{BC} versus $M(\pi^+\pi^-)$ of the DT candidate in (a) data and (b) the 2D fit result, where the black dots with error bars are data, the blue solid curves are the fit results, the red-dashed lines are signal function, the black-dashed lines are background neither peaking in the $M(\pi^+\pi^-)$ distribution nor the M_{BC} distribution, the green-dotted lines are background peaking around the Λ_c^- mass in the M_{BC} distribution, and the cyan-dash-dotted lines are background peaking around the K_S^0 mass in the $M(\pi^+\pi^-)$ distribution.

We refer to the systematic uncertainty for $\sum N_i^{\text{tag}}$. $\epsilon_i^{\text{tag,sig}}/\epsilon_i^{\text{tag}}$ as ST-related systematic uncertainty. The systematic uncertainty of the ST yields (N_i^{tag}) is studied by altering the signal shape, fitting range, and end point of the ARGUS function. The uncertainty due to limited MC statistics is taken as the uncertainty of the ST and DT efficiencies (ϵ_i^{tag} and $\epsilon_i^{\text{tag,sig}}$). The total relative ST-related systematic uncertainty is calculated to be 1.2%. The systematic uncertainty of the K_S^0 reconstruction is determined to be 1.5% by studying control samples of $J/\psi \rightarrow K^{*\mp}K^\pm$ and $J/\psi \rightarrow \phi K_S^0 K^\pm \pi^\mp$ and weighting over the momentum of the K_S^0 [24]. The systematic uncertainty for $\mathcal{B}(K_S^0 \rightarrow \pi^+\pi^-)$ is 0.1% from PDG [2]. The systematic uncertainty of the signal yield is estimated by altering the K_S^0 signal function, background function and the 2D fit range, The relative changes (3.4%) in the BF are taken as systematic uncertainties. Assuming no correlations between sources, the total systematic uncertainty is obtained as the sum in quadrature.

TABLE III. Systematic uncertainties in the measurement of the BF of $\Lambda_c^+ \rightarrow K_S^0 X$.

Source	Uncertainty (%)
ST related	1.2
K_S^0 reconstruction	1.5
$\mathcal{B}(K_S^0 \rightarrow \pi^+\pi^-)$	0.1
Signal yield	3.4
Total	3.9

In summary, the absolute BF of the inclusive decay $\Lambda_c^+ \rightarrow K_S^0 X$ is measured for the first time by using an e^+e^- data sample of 567 pb^{-1} taken at $\sqrt{s} = 4.6 \text{ GeV}$ with the BESIII detector. The result is $\mathcal{B}(\Lambda_c^+ \rightarrow K_S^0 X) = (9.9 \pm 0.6 \pm 0.4)\%$, where the first uncertainty is statistical and the second systematic. The BF of the inclusive decay $\Lambda_c^+ \rightarrow \bar{K}^0/K^0 X$ is $(19.8 \pm 1.2 \pm 0.8 \pm 1.0)\%$ where the third uncertainty of $\pm 5\%$ is included to account for possible differences between $\mathcal{B}(\Lambda_c^+ \rightarrow K_S^0 X)$ and $\mathcal{B}(\Lambda_c^+ \rightarrow K_L^0 X)$ [25], which is consistent with calculations with the statistical isospin model within 1.3σ . The relative BF deviation of $(18.7 \pm 8.3)\%$ between the inclusive \bar{K}^0/K^0 decay and the observed exclusive decays of Λ_c^+ , can be addressed by the extrapolated exclusive decays of Λ_c^+ listed in Table I. Experimentally, only one decay mode involving a neutron in the final state was observed at BESIII [9]. More decay modes involving neutrons or hyperons in the final states can be experimentally pursued, especially decays with a large BF, e.g. $\Lambda_c^+ \rightarrow n \bar{K}^0 \pi^+ \pi^0$ whose BF is calculated to be $(3.07 \pm 0.16)\%$ by the statistical isospin model. Recently, the BF of $\Lambda_c^+ \rightarrow \Xi^0 K^0 \pi^+$ was calculated to be $(8.70 \pm 1.70)\%$ by the SU(3) flavor symmetry model [26], while it is only $(0.62 \pm 0.06)\%$ in the statistical isospin model. Measuring the BF of $\Lambda_c^+ \rightarrow \Xi^0 K^0 \pi^+$ will test these two models.

The BESIII collaboration thanks the staff of BEPCII and the IHEP computing center for their strong support. This work is supported in part by National Key Basic Research Program of China under Contract No. 2015CB856700; Chinese Academy of Science Focused Science Grant; National 1000 Talents Program of China; National Natural Science Foundation of China (NSFC) under Contracts Nos. 11905225, 11775230, 11935018, 11625523, 11635010, 11735014, 11822506, 11835012, 11935015, 11935016, 11521505, 11425524, 11605042, 11961141012; the Chinese Academy of Sciences (CAS) Large-Scale Scientific Facility Program; Joint Large-Scale Scientific Facility Funds of the NSFC and CAS under Contracts Nos. U1732263, U1832207; CAS Key Research Program of Frontier Sciences under Contracts Nos. QYZDJ-SSW-SLH003, QYZDJ-SSW-SLH040; 100 Talents Program of CAS; INPAC and Shanghai Key Laboratory for Particle Physics and Cosmology; ERC under Contract No. 758462; German Research Foundation DFG under Contracts Nos. Collaborative Research Center CRC 1044, FOR 2359; Istituto Nazionale di Fisica Nucleare, Italy; Ministry of Development of Turkey under Contract No. DPT2006K-120470; National Science and Technology fund; STFC (United Kingdom); The Knut and Alice Wallenberg Foundation (Sweden) under Contract No. 2016.0157; The Royal Society, UK under Contracts Nos. DH140054, DH160214; The Swedish Research Council; U. S. Department of Energy under Contracts Nos. DE-FG02-05ER41374, DE-SC-0010118, DE-SC-0012069.

-
- [1] G. S. Abrams *et al.* (Mark II Collaboration), Phys. Rev. Lett. **44**, 10 (1980).
- [2] M. Tanabashi *et al.* (Particle Data Group), Phys. Rev. D **98**, 030001 (2018) and 2019 update.
- [3] M. Ablikim *et al.* (BESIII Collaboration), Phys. Rev. Lett. **115**, 221805 (2015).
- [4] M. Ablikim *et al.* (BESIII Collaboration), Phys. Rev. Lett. **116**, 052001 (2016).
- [5] M. Ablikim *et al.* (BESIII Collaboration), Phys. Rev. Lett. **117**, 232002 (2016).
- [6] M. Ablikim *et al.* (BESIII Collaboration), Phys. Lett. B **767**, 42 (2017).
- [7] M. Ablikim *et al.* (BESIII Collaboration), Phys. Lett. B **783**, 200 (2018).
- [8] M. Ablikim *et al.* (BESIII Collaboration), Phys. Rev. D **99**, 032010 (2019).
- [9] M. Ablikim *et al.* (BESIII Collaboration), Phys. Rev. Lett. **118**, 112001 (2017).
- [10] M. Ablikim *et al.* (BESIII Collaboration), Phys. Lett. B **772**, 388 (2017).
- [11] M. Gronau and J. L. Rosner, Phys. Rev. D **97**, 116015 (2018); Addendum: Phys. Rev. D **98**, 073003 (2018).
- [12] M. Ablikim *et al.* (BESIII Collaboration), Phys. Rev. Lett. **121**, 062003 (2018).
- [13] M. Ablikim *et al.* (BESIII Collaboration), Chin. Phys. C **39**, 093001 (2015).
- [14] R. M. Baltrusaitis *et al.* (MARK-III Collaboration), Phys. Rev. Lett. **56**, 2140 (1986).
- [15] M. Ablikim *et al.* (BESIII Collaboration), Nucl. Instrum. Methods Phys. Res., Sect. A **614**, 345 (2010).
- [16] S. Agostinelli *et al.* (GEANT4 Collaboration), Nucl. Instrum. Methods Phys. Res., Sect. A **506**, 250 (2003).
- [17] E. A. Kuraev and V. S. Fadin, Yad. Fiz. **41**, 733 (1985) [Sov. J. Nucl. Phys. **41**, 466 (1985)].
- [18] E. Richter-Was, Phys. Lett. B **303**, 163 (1993).
- [19] S. Jadach, B. F. L. Ward and Z. Was, Comp. Phys. Commun. **130**, 260 (2000); Phys. Rev. D **63**, 113009 (2001).
- [20] R. G. Ping, Chin. Phys. C **32**, 599 (2008); D. J. Lange, Nucl. Instrum. Methods Phys. Res., Sect. A **462**, 152 (2001).
- [21] J. C. Chen, G. S. Huang, X. R. Qi, D. H. Zhang, and Y. S. Zhu, Phys. Rev. D **62**, 034003 (2000).
- [22] X. Y. Zhou, S. X. Du, G. Li, and C. P. Shen, arXiv:2001.04016v1.
- [23] H. Albrecht *et al.* (ARGUS Collaboration), Phys. Lett. B **241**, 278 (1990).
- [24] M. Ablikim *et al.* (BESIII Collaboration), Phys. Rev. D **92**, 112008 (2015).
- [25] I. I. Bigi, H. Yamamoto, Phys. Lett. B **349**, 363 (1995).
- [26] C. Q. Geng, Y. K. Hsiao, Chia-Wei Liu, and Tien-Hsueh Tsai, Phys. Rev. D **99**, 073003 (2019).